

# First-principles study of the geometric and electronic structure of Au<sub>13</sub> clusters: Importance of the prism motif

Mathis Gruber,<sup>1,2</sup> Georg Heimel,<sup>2,\*</sup> Lorenz Romaner,<sup>1</sup> Jean-Luc Brédas,<sup>2</sup> and Egbert Zojer<sup>1,†</sup>

<sup>1</sup>*Institute of Solid State Physics, Graz University of Technology, Petersgasse 16, A-8010 Graz, Austria*

<sup>2</sup>*School of Chemistry and Biochemistry and Center for Organic Photonics and Electronics, Georgia Institute of Technology, 901 Atlantic Drive, NW, Atlanta, Georgia 30332-0400, USA*

(Received 13 July 2007; revised manuscript received 21 September 2007; published 9 April 2008)

The geometric structure, symmetry, and spin of Au<sub>13</sub> clusters are investigated in the framework of density-functional theory, with particular attention paid to the correlation among these properties. Several computational approaches are carefully tested on previously proposed cluster configurations. Complications and possible pitfalls in electronic-structure calculations on these systems are highlighted. Using molecular dynamics with quantum mechanically calculated forces, a set of favored (high binding energy) geometric structures, where a trigonal prism acts as the central building block, is discussed.

DOI: 10.1103/PhysRevB.77.165411

PACS number(s): 61.46.Df, 61.43.Bn, 73.22.-f, 36.20.Hb

## I. INTRODUCTION

The exact nature of the geometric structure of small gold clusters remains controversial.<sup>1–8</sup> However, as the structure strongly impacts their electronic properties,<sup>9–13</sup> good models are needed to explore potential applications that rely on the chemical reactivity of these clusters.<sup>14–16</sup> The 13-atom cluster, Au<sub>13</sub>, has received particular attention, as this “magic number” corresponds to the first geometric shell closing for both icosahedral and cuboctahedral structures.<sup>17</sup> These highly symmetrical configurations are also the two most frequently studied structures for Au<sub>13</sub>.<sup>3,18–21</sup> The current view is that, while both are local minima in the potential-energy surface (PES) with the cuboctahedron significantly favored in energy over the icosahedron, many isomers with higher binding energy exist. In fact, Au<sub>13</sub> appears to be near the critical cluster size where a transition from preferentially planar [two dimensional (2D)] to more compact, quasispherical [three dimensional (3D)] structures occurs.<sup>1,2,4,6,8,22–24</sup> Compared to other metals,<sup>25</sup> 2D structures are energetically favored up to larger cluster sizes in gold due to the importance of relativistic effects.<sup>8,11,18–20,24,26</sup> Consequently, a number of planar and amorphous configurations have been proposed to be energetically at or near the most stable structure.<sup>1,2,4,5,8,13,22–25</sup> Moreover, it has been shown recently that the structure with the highest binding energy is not the only one of practical relevance, since dynamic and entropic effects need to be considered as well, when evaluating the probability of finding small Au clusters in certain configurations. These effects can make 3D clusters of somewhat lower binding energies more probable,<sup>27</sup> highlighting the need for a systematic classification scheme for high binding-energy 3D clusters.

Here, we first discuss the impact of the Fermi-smearing parameter<sup>28,29</sup> (used in fractional orbital-occupancy computational schemes) on the  $z$  component of the total spin ( $S_z$ ) of Au<sub>13</sub> and its interplay with the geometric structure. For the sake of comparison with previous investigations, we also study the impact of various types of basis function used to expand the valence Kohn-Sham orbitals in electronic-structure calculations of Au<sub>13</sub> clusters. Finally, we describe the results of molecular dynamics simulations with quantum

mechanically calculated forces (MD/QM), which uncover a prism-type structural pattern that allows a systematic design of high binding-energy 3D configurations. Considering the above discussed aspects, these can be expected to be of particular relevance for small Au clusters and should have implications also for other metals.

## II. METHODOLOGY

Spin-polarized calculations were performed at the density-functional theory (DFT) level with the SIESTA code.<sup>30</sup> Unless otherwise mentioned, a double-zeta basis set including polarization functions (DZP), the PBE exchange-correlation (XC) functional,<sup>31</sup> and norm-conserving pseudopotentials (including scalar relativistic effects) according to the Troullier-Martin scheme were used<sup>32,33</sup> (cutoff radii  $r_c$  were set to 2.3, 2.3, 1.5, and 1.8 bohr for the  $s$ ,  $p$ ,  $d$ , and  $f$  orbitals, respectively). The equivalent plane-wave cutoff for the fast Fourier transform grid (mesh cutoff) was set to 170 Ry (increasing the mesh cutoff to 300 Ry in test calculations changed the relative binding energies by only 0.1 meV/atom). The Fermi-Dirac occupation function with an electronic temperature of 0.01 eV was used;<sup>28</sup> this choice guaranteed a correct description of the  $z$  component of the spin,  $S_z$  (*vide infra*), and a stable self-consistent field (SCF) convergence behavior. In order to limit the extent of the pseudoatomic orbitals (PAOs) used as basis functions, we applied a PAO energy shift of 34 meV and truncated the orbitals at the resulting radial node.<sup>30</sup> The relative tolerance in the density matrix (DM), taken as SCF convergence criterion, was set to  $10^{-4}$ . All geometries were converged until forces were smaller than 0.01 eV/Å. No explicit symmetry constraints were imposed. A cubic unit cell of  $20 \times 20 \times 20$  Å was sufficient to electronically isolate periodic images of the cluster. For the sake of comparison, additional calculations were performed with VASP (Refs. 34–39) and GAUSSIAN98.<sup>40</sup> Details and parameters for all DFT codes used are shown in Table I.

As straightforward minimization schemes are insufficient to probe the complex PES of the Au<sub>13</sub> cluster, we employed a two-step procedure: The first step is a scan of the PES,

TABLE I. Summary of the relevant parameters in the density-functional codes used in the present study. See Sec. II for details; in the GAUSSIAN98 calculations, apart from the specific details given below, only default parameters have been used.

	SIESTA	VASP	GAUSSIAN98
<i>Basis functions</i>	DZP	Plane-waves cutoff=300 eV	SDD <sup>a</sup> and LANL2DZ <sup>b</sup>
<i>XC functional</i>	PBE	PW91 <sup>c</sup>	B3PW91 <sup>c,d</sup>
<i>Occupation function</i>	Fermi-Dirac	Fermi-Dirac	
<i>Electronic temperature</i>	0.01 eV	0.01 eV	
<i>PAO energy shift</i>	34 meV		
<i>Unit-cell size</i>	20 Å	20 Å	
<i>Mesh cutoff</i>	170 Ry	450 eV	default
<i>DM tolerance</i>	10 <sup>-4</sup>	10 <sup>-4</sup>	10 <sup>-6</sup>
<i>Force tolerance</i>	0.01 eV/Å	0.01 eV/Å	0.023 eV/Å
<i>Pseudopotential</i>	Troullier-Martin norm conserving	Projector <sup>c</sup> augmented waves	SDD <sup>a</sup> and LANL2DZ <sup>b</sup> (matching basis set)

<sup>a</sup>Reference 44.

<sup>b</sup>References 45–47.

<sup>c</sup>References 49 and 50.

<sup>d</sup>Reference 51.

<sup>e</sup>References 34 and 39.

achieved via MD/QM simulations using SIESTA. In the second step, selected potential-energy minima (i.e., maxima in binding energy) of the MD/QM simulations are used as starting structures for a conjugate-gradient (CG) geometry optimization, leading to fully relaxed structures. For the MD/QM simulations, the Verlet algorithm<sup>41</sup> was chosen with a discrete time step of 15 fs. Test calculations with time steps as low as 3 fs yielded equivalent results. The starting temperature was set to 1000 K and various 3D starting structures were tested. All minima with total energies lower (binding energies higher) than the cuboctahedral configuration were considered as starting structures for CG geometry optimizations.

### III. RESULTS AND DISCUSSION

#### A. Spin, structure, and fractional-occupancy schemes

As gold has 79 electrons (11 valence electrons treated explicitly), the total spin of a Au<sub>13</sub> cluster, or rather its projection onto a unique axis,  $S_z$ , has to be a multiple of 1/2 (neglecting spin-orbit coupling,<sup>18,20</sup> which has been shown not to affect the relative stability of different cluster morphologies at least when treated in a perturbation approach<sup>24</sup>). For all nonsymmetric structures, we find  $S_z=1/2$  as, according to Hund's rule, higher  $S_z$  values are possible only when the highest occupied orbitals are degenerate. Possible degeneracies are determined by the cluster symmetry, i.e., by the dimensionality of the irreducible representations in the cluster point group. For 2D cluster structures, only one highly symmetric configuration is conceivable: a star-shaped cluster ( $D_{6h}$ ) with at most twofold degenerate orbitals.<sup>4</sup> An odd number of electrons still leads to only  $S_z=1/2$ . We therefore find  $S_z=1/2$  for all planar Au<sub>13</sub> clusters.

The fully symmetric (*vide infra*) cuboctahedral cluster belongs to the  $O_h$  point group, containing various two- and threefold degenerate irreducible representations. In principle, both 1/2 and 3/2 are thus possible values for  $S_z$ . Since the highest occupied orbital is threefold degenerate and has to accommodate five electrons, the  $S_z=3/2$  solution can be ruled out leaving  $S_z=1/2$  as the expected  $z$  component for the spin in the cuboctahedron. The fully symmetric (*vide infra*) icosahedral cluster belongs to the  $I_h$  point group, which contains three-, four-, and fivefold degenerate irreducible representations leading to 1/2, 3/2, and 5/2 as possible  $S_z$  values. The highest occupied orbital is fivefold degenerate and filled with five electrons; thus,  $S_z=5/2$  in accordance with Hund's rule.

While these findings are hardly surprising, we emphasize that care must be taken in standard DFT calculations on these structures in order to obtain correct results. It is common practice in many DFT codes (e.g., VASP or SIESTA) to use a Fermi-smearing scheme (i.e., fractional occupancy of frontier orbitals) to improve the convergence behavior in the SCF cycle for metallic structures.<sup>28,29</sup> In systems where unoccupied orbitals of the opposite spin manifold are present close to the Fermi level, however, these partial-occupancy schemes can erase the spin information in the calculation (Fig. 1). In fact, for the icosahedral cluster, we find  $S_z=5/2$  only when small enough electronic temperatures are considered (i.e., a Fermi smearing of 0.01 eV in our calculations); in this case, of the five degenerate orbitals around the Fermi level ( $E_F$ ), the occupied spin-up manifold [Fig. 1(a)] is energetically stabilized (shifted below  $E_F$ ) relative to the unoccupied spin-down manifold (which is shifted above  $E_F$ ). Raising the electronic temperature to 0.2 eV (a typical value used for metals) increases the occupancy of the spin-down states and the situation depicted in Fig. 1(b) is eventually reached: Each of the

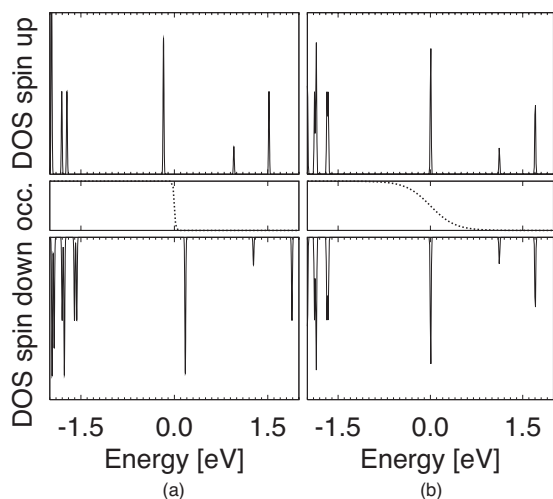


FIG. 1. Spin-polarized density of states around the Fermi level (set at 0.0 eV) for the relaxed, fully symmetric icosahedral  $\text{Au}_{13}$  cluster with electronic temperatures of (a) 0.01 and (b) 0.2 eV. The occupation function (Fermi-Dirac) is indicated in the middle panels.

five spin-up and spin-down orbitals (now all at  $E_F$ ) contains 0.5 electrons and the spin-unpolarized solution (with  $S_z=0$ ) is obtained. This results in a complete loss of information on the spin properties.

The actually chosen value of the Fermi smearing is also linked to the details of the cluster geometry as is discussed for the cuboctahedral cluster in the following: For a high electronic temperature (0.2 eV) or equivalency for a spin-unpolarized calculation  $S_z=0$  is obtained and the CG-optimized structure is virtually symmetric. For this geometry and close to zero Fermi smearing (actually 1 meV for convergence reasons) one obtains a threefold degenerate level in the spin-up manifold right at  $E_F$ , where each of the degenerate spin up orbitals contains  $2/3$  of an electron (see Fig. 2(a)). This results in a correct value of  $S_z=1/2$ . For zero Fermi smearing, the “exactly” cuboctahedral symmetry is, however, not a local minimum as inferred from the residual forces obtained at that geometry. Slightly breaking the cuboctahedral symmetry of the starting geometry then indeed results in a somewhat distorted configuration of the CG-optimized cluster. The degeneracy of the spin-down levels is lifted as two orbitals of the threefold degenerate level become fully occupied and are energetically stabilized (see Fig. 2(b)). In that case, also no convergence problems for a Fermi smearing of 0 meV are observed. For sufficiently small Fermi smearings, we thus find that (in the absence of spin-orbit coupling) the cuboctahedral cluster undergoes static Jahn-Teller distortion<sup>42</sup> while the icosahedral structure remains perfectly symmetric. Intriguingly, relativistic studies employing double point-group orbital symmetries suggest that the opposite should be the case.<sup>18</sup>

For the other cluster structures discussed below, we also found that the fully relaxed geometries can slightly change upon varying the electronic temperature, especially if it is chosen too high. In the remainder of the manuscript a smearing of 0.01 eV was used (test calculations with zero Fermi smearing yielded essentially the same result apart from the

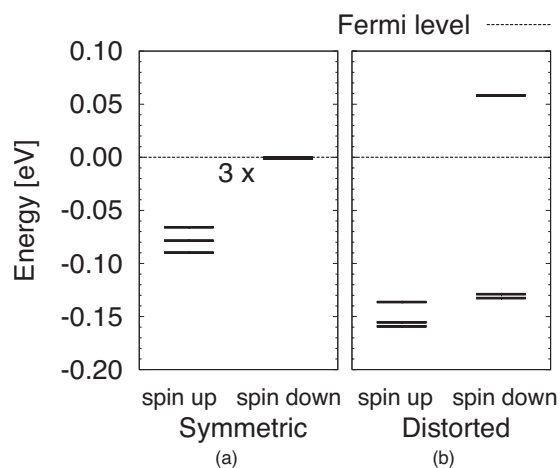


FIG. 2. Orbital energies for (a) the relaxed virtually symmetric cuboctahedron and (b) for the Jahn-Teller distorted cuboctahedron. The orbital degeneracy in the spin-down manifold around the Fermi level (dotted horizontal line) is lifted in (b). We note that due to convergence problems in the SCF procedure caused by orbital degeneracy, a Fermi smearing of 1 meV had to be used for the symmetric cluster, while it was set to 0 meV in the broken symmetry case.

case of the cuboctahedral cluster discussed above. A thorough discussion on how fractional occupancies of orbitals affects gradients to the total energy especially when degeneracies are involved can also be found in Ref. 43.

## B. Impact of the basis set (linear combination of atomic orbitals vs plane wave)

In order to achieve a reliable description of the geometric structure of  $\text{Au}_{13}$  clusters, we chose to reexamine several cluster configurations with high binding energy that have been proposed earlier.<sup>23</sup> In particular, we considered the planar (2D) structures as well as the most stable 3D cluster proposed by Xiao *et al.*<sup>23</sup> Following their notation, these will be labeled  $P_{13-1}$  through  $P_{13-4}$  and  $T_{13-1}$ , respectively.

Xiao *et al.*<sup>23</sup> carried out their calculations with the VASP code, which employs plane waves to expand the Kohn-Sham orbitals of the valence electrons. This is in contrast to the linear combination of atomic orbitals (LCAO) approach used in SIESTA. In order to get a better understanding of the impact of the basis set, we therefore recalculated the  $P_{13-1}$  through  $P_{13-4}$  and  $T_{13-1}$  cluster configurations with VASP. For the sake of completeness, the two limiting cases ( $P_{13-1}$  and  $T_{13-1}$ ) were also calculated with GAUSSIAN98, a nonperiodic quantum-chemistry code also employing LCAO.

In Fig. 3, we show the results of our calculations in comparison to the values from Ref. 23. In addition to the parameters listed in Table I, we undertook numerous tests: VASP calculations with an alternative plane-wave cutoff of 500 eV and calculations with the PBE XC functional<sup>31</sup> were performed. SIESTA calculations with an increased mesh cutoff of 300 Ry and calculations using a softer potential ( $r_c=2.5, 3.0, 2.0$ , and 2.0 bohr for the  $s, p, d$ , and  $f$  orbitals, respectively) were undertaken. The corresponding variations are indicated

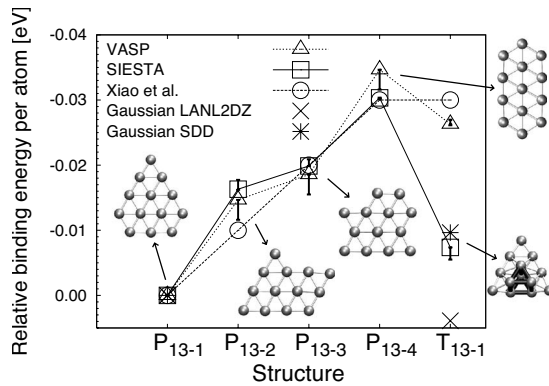


FIG. 3. Binding energies per atom (in eV) for several planar (2D) clusters ( $P_{13-1}$  through  $P_{13-4}$ ) and a 3D cluster ( $T_{13-1}$ ) relative to the binding energy per atom of the  $P_{13-1}$  cluster. Results are shown for LCAO (SIESTA and GAUSSIAN98) and plane-wave (VASP) basis sets and compared to literature values from Ref. 23. The latter were unfortunately given only to two significant digits, which is one of the reasons for the small deviations in the trend compared to our VASP calculations. The error bars indicate the variations resulting from testing different computational parameters in the respective DFT codes.

with error bars and do not affect the obtained trends.

Our VASP calculations, as expected, reproduce the trends given by Xiao *et al.*<sup>23</sup> while the GAUSSIAN98 results (with both available pseudopotential and basis-set combinations, SDD<sup>44</sup> and LANL2DZ<sup>45-47</sup>) follow the trends of the SIESTA calculations (interestingly, also when including exact exchange). The main deviation between the results obtained by Xiao *et al.*<sup>23</sup> (and our VASP calculations) and those calculated with SIESTA (and GAUSSIAN98) is that the difference in binding energy between  $P_{13-1}$  and  $T_{13-1}$  is about four times higher for the former [ $\Delta E = E(P_{13-1}) - E(T_{13-1}) \approx 30$  meV] than for the latter [ $\Delta E = E(P_{13-1}) - E(T_{13-1}) \approx 7$  meV].

Since both SIESTA and GAUSSIAN98 use LCAOs as basis functions, while VASP uses plane-wave-type functions, it appears that the *type* of basis functions could be responsible for the differences [especially since the code dependent differences are much larger than those originating, e.g., from different pseudopotentials (*vide supra*)]. A possible explanation for our observations could be that the quality of the plane-wave basis set is independent of the topology (i.e., 2D or 3D) of the system. For LCAO basis functions, the situation is different; the atomic orbitals are centered on individual atoms and the quality of the “overall” basis set depends on the positions of the atoms relative to each other (a situation reminiscent of the basis-set superposition error). This implies that the relatively lower binding energy (larger total energy) for the 2D clusters provided by SIESTA (and GAUSSIAN98) could be a consequence of the lower “effective quality” of the basis set for systems that are more extended in two dimensions (2D conformations having a larger surface to volume ratio) compared to the more compact quasispherical structures.

As a next step, we will perform a thorough configurational search, which can be most efficiently done using the LCAO code SIESTA, and will then revisit the issue of plane-

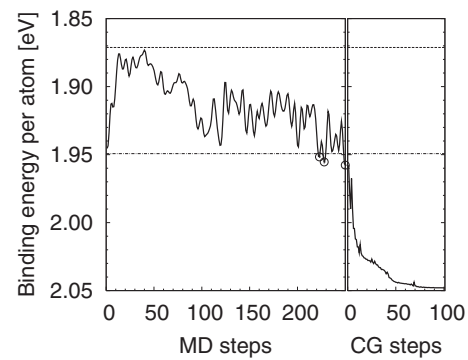


FIG. 4. Illustration of the computational scheme used to scan the potential-energy surface of  $Au_{13}$ : sample MD/QM calculation (left panel) and subsequent CG geometry optimization of one of the local minima (right panel). The binding energy per atom (in eV) in the course of the MD/QM run typically fluctuates between the values for the icosahedral (top horizontal line) and the cuboctahedral (bottom horizontal line) structures. All local minima with a higher binding energy than the cuboctahedron (marked by circles) are forwarded to a CG geometry optimization (here, shown for the last minimum in the MD/QM run).

wave type vs LCAO based calculations at the end of the next section.

### C. Prism structures

When following the approach described in Sec. II to scan the PES, various structures with a higher binding energy than the cuboctahedral cluster can be identified. Figure 4 illustrates a sample MD/QM run together with the subsequent CG optimization of one of the local energy minima (maxima in binding energy).

The binding energies of the cluster configurations found in this way are shown in Fig. 5 and they fall into three groups. The geometric structures of the highest binding-energy configurations are shown in Fig. 6 (framed structures). They systematically exhibit one specific geometrical pattern (see highlighted bonds in Fig. 6) corresponding to a

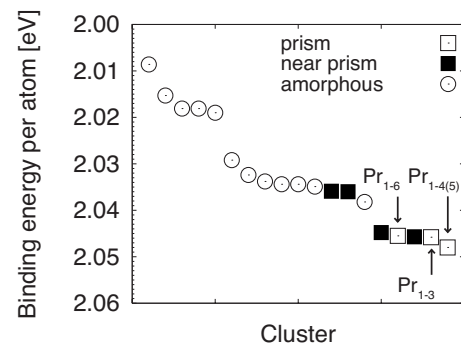


FIG. 5. Binding energies per atom for a series of cluster structures obtained through the procedure outlined in the text. The values for the icosahedral (1.87 eV) and cuboctahedral (1.95 eV)  $Au_{13}$  clusters are outside the displayed range. Three groups can be distinguished: amorphous (left), near prism (center), and prism (right).

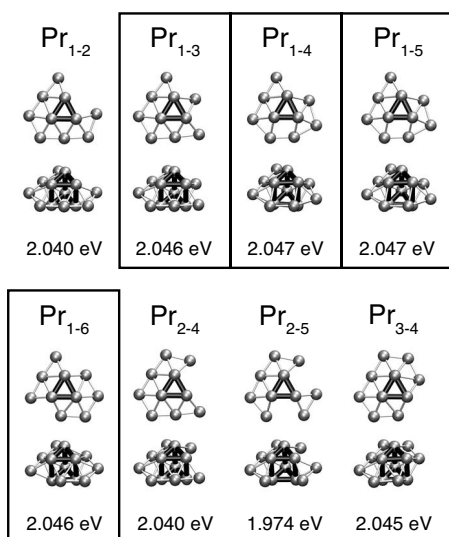


FIG. 6. Structures and binding energies per atom for the eight prism clusters (top and side views). The trigonal prism is highlighted. The framed structures were found by scanning the potential-energy surface using the MD/CG procedure described in Sec. II, while the remaining structures were constructed from the 15-atom parent cluster. See text for details.

trigonal prism; they will, therefore, be referred to in the following as *prism structures*. We find (Fig. 5) slightly modified prism structures very close in energy and at lower binding energies a group of “amorphous” structures that neither contain the prism motif nor exhibit any other systematic pattern. The fact that none of the 2D clusters is found by the MD runs can be attributed to the 3D starting geometries and the high potential-energy barriers that need to be overcome between 2D and 3D structures.<sup>27</sup> The potential range of 2D clusters can, however, be easily scanned “by hand” as done in Ref. 23. Their binding energies relative to the prism structures will be discussed below after a systematic assessment of the prism motif.

We find that the trigonal prism in the center of the prism structures is neither perfect nor exactly the same in each structure. Due to different positions of the surrounding atoms (Fig. 6), the bond lengths of the sides of the triangles vary from 2.73 to 2.84 Å and the height of the prism from 2.89 to 3.48 Å. The (partial) ring (atoms *not* connected by highlighted bonds in Fig. 6) is almost planar, lies parallel to the triangular faces, and bisects the height of the prism. While the shape of the ring is different in each cluster, the minimum distances to the nearest prism atoms are similar and vary only from 2.81 to 2.93 Å. Furthermore, as can be seen in the top views in Fig. 6, no more than three Au atoms are attached to any side of the triangles.

From these Au<sub>13</sub> structures, an obvious Au<sub>15</sub> parent structure can be designed (see Fig. 7) with a ring of nine equidistant Au atoms placed around the central prism. By removing two atoms from the ring, a total of eight symmetry inequivalent Au<sub>13</sub> clusters can then be derived. They are denoted as Pr<sub>*i-j*</sub>, where *i* and *j* indicate the free positions in the ring according to Fig. 7. Choosing starting structures with 2.9 Å for the height and side lengths of the prism and 3.77 Å for

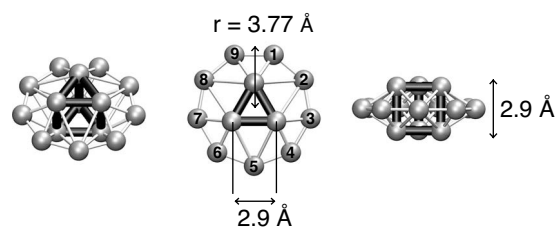


FIG. 7. The 15-atom parent cluster used to construct the 13-atom prism structures discussed in the present study.

the radius of the ring, we performed CG geometry optimizations on all eight inequivalent prism clusters. For the four structures already found through the MD/QM procedure, Pr<sub>1-3</sub> through Pr<sub>1-6</sub> (Fig. 6), the binding energies from the MD/QM//CG run are reproduced. The four additional prism configurations have very similar binding energies; in fact, the inequivalent Pr<sub>1-2</sub> and Pr<sub>2-4</sub> (as well as Pr<sub>1-4</sub> and Pr<sub>1-5</sub>) starting geometries result in the same converged cluster structures. All prism structures and their binding energies are collected in Fig. 6.

We note that some of the prism structures have been observed previously [in particular, Pr<sub>1-4</sub> (Refs. 5 and 48) and Pr<sub>3-4</sub> (Refs. 8 and 48)] but were classified as stable amorphous structures, thereby overlooking the common prism motif. Also, the 3D cluster with the highest binding energy described in Refs. 1, 4, and 23, *T*<sub>3-1</sub>, is, in fact, a slightly modified prism structure; it can be constructed by moving the atom in the 2-position of the Pr<sub>1-3</sub> structure (Fig. 6) to the opposite side (see Fig. 8). Energetically, we find the binding energy in the *T*<sub>3-1</sub> cluster to be only marginally lower (~5 meV/at.) than in our lowest-energy prism cluster (Pr<sub>1-4</sub>). When revisiting the suggested stable structures for neutral and anionic 12-, 14-, and 15-atom gold clusters, a central prism surrounded by the remaining atoms can be identified as well.<sup>1,4,22,23</sup> It thus appears that this motif is an important structural pattern for intermediately sized Au<sub>*n*</sub>

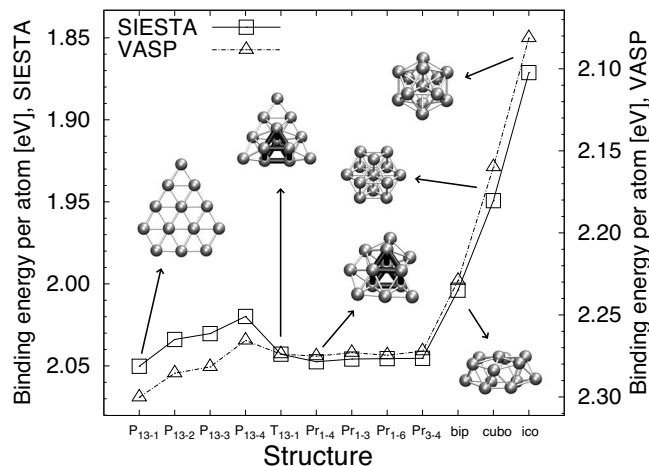


FIG. 8. Comparison of the binding energies per atom (in eV) in different cluster structures obtained with LCAO (SIESTA) and plane-wave (VASP) basis functions. The left (SIESTA) and right (VASP) energy axes have been vertically shifted so that the results for the *T*<sub>3-1</sub> cluster overlap.

clusters ( $n$  around 13) while planar cluster are preferred for lower  $n$ ,<sup>1,2,4,6,8,22,24,26</sup> and more compact spherical structures become dominant with increasing cluster size.<sup>3,7,9,11</sup>

In Fig. 8, we summarize our findings by comparing the binding energies of all clusters we investigated so far: (i) the highest binding-energy planar structures ( $P_{13-1}$  to  $P_{13-4}$ ) discussed in Ref. 23; (ii)  $T_{13-1}$  as the highest binding-energy 3D structure from that work; (iii) selected prism structures; and (iv) the highly symmetric cuboctahedral and icosahedral structures discussed in Sec. III A. In addition, the biplanar structure proposed by Chang and Chou<sup>25</sup> is included. The prismlike and planar structures clearly display the highest binding energies. Revisiting the question of the basis functions used to expand the valence Kohn-Sham orbitals, we note that the absolute binding energies calculated with VASP are systematically higher. The relative trends for the binding energies within the classes of prism and/or biplanar and planar clusters are essentially the same for both LCAO (SIESTA) and plane-wave-type (VASP) approaches. In the former case, however, the class of planar clusters is somewhat destabilized, supporting our hypothesis that the quality of the LCAO basis set is effectively lower for planar structures.

Independent of the choice of basis set, it can be concluded that prism and 2D clusters are very close in energy, which is consistent with  $Au_{13}$  being at the border line between 2D and 3D structures.<sup>1,4,6,8,22,23,27,48</sup> It is interesting to note that, even if certain 2D clusters are energetically more stable, the considerations given in Ref. 27 imply that higher dimensionality clusters should be the most common conformation of  $Au_{13}$  due to dynamic and entropic reasons. This underlines the practical relevance of the class of prism-type clusters discussed here.

#### IV. SYNOPSIS

We have discussed the dependence of the spin multiplicity of  $Au_{13}$  clusters on their structure, finding  $S_z=5/2$  for the

icosahedral structure and  $S_z=1/2$  for the cuboctahedral and all other planar (2D) or amorphous 3D structures. The critical impact that the Fermi-smearing parameter in fractional-occupancy schemes can have on the calculations of the spin and structural properties is highlighted; it turns out that particular care must be taken to choose the electronic temperature low enough so as to maintain the correct spin state; a too large Fermi smearing is shown to result in a complete loss of information on spin.

Using a combination of MD/QM calculations with CG optimizations to scan the potential-energy surface of  $Au_{13}$  clusters, we have uncovered a class of low-energy structures which can be systematically constructed by using a trigonal prism as the basic building block. The binding energies of these structures are close to those of 2D clusters, which have previously been suggested to be the most stable conformers of  $Au_{13}$ .<sup>23</sup> The actual energetic order is found to depend on the applied methodology with plane-wave-type basis sets somewhat favoring planar structures. This notwithstanding, the entropic and dynamic effects discussed in Ref. 27 make prism-type clusters highly relevant and potentially the most common type of  $Au_{13}$  clusters.

#### ACKNOWLEDGMENTS

GH is a Marie-Curie fellow under the INSANE project (OIF Contract No. 021511). Financial support by Project No. N-702-SENSPYS of the Austrian Nano-initiative and the SFB Electroactive Stoffe (Project No. F917) is gratefully acknowledged. The work at Georgia Tech has been partly supported by the National Science Foundation (under the STC program, Award No. DMR-0120967, and the CRIF program, Award No. CHE-0443564) and the Office of Naval Research. The authors are also grateful to O. Kwon and H. Krenn for stimulating discussions and the section “Computing & Application Services” of the Zentrale Informatikdienst of the Graz University of Technology for providing computational resources.

\*georg.heimel@physik.hu-berlin.de

†egbert.zoer@tugraz.at

<sup>1</sup>F. Furche, R. Ahlrichs, P. Weis, C. Jacob, S. Gilb, T. Bierweiler, and M. M. Kappes, *J. Chem. Phys.* **117**, 6982 (2002).

<sup>2</sup>S. Gilb, P. Weis, F. Furche, R. Ahlrichs, and M. M. Kappes, *J. Chem. Phys.* **116**, 4094 (2002).

<sup>3</sup>O. D. Häberlen, S. C. Chung, M. Stener, and N. Rösch, *J. Chem. Phys.* **106**, 5189 (1997).

<sup>4</sup>H. Häkkinen, B. Yoon, U. Landman, X. Li, H. J. Zhai, and L. S. Wang, *J. Phys. Chem. A* **107**, 6168 (2003).

<sup>5</sup>J. Oviedo and R. E. Palmer, *J. Chem. Phys.* **117**, 9548 (2002).

<sup>6</sup>J. L. Wang, G. H. Wang, and J. J. Zhao, *Phys. Rev. B* **66**, 035418 (2002).

<sup>7</sup>N. T. Wilson and R. L. Johnston, *Eur. Phys. J. D* **12**, 161 (2000).

<sup>8</sup>E. M. Fernandez, J. M. Soler, I. L. Garzon, and L. C. Balbas, *Phys. Rev. B* **70**, 165403 (2004).

<sup>9</sup>I. L. Garzon, K. Michaelian, M. R. Beltran, A. Posada-Amarillas, P. Ordejon, E. Artacho, D. Sanchez-Portal, and J. M.

Soler, *Eur. Phys. J. D* **9**, 211 (1999).

<sup>10</sup>E. Gutierrez, R. D. Powell, F. R. Furuya, J. F. Hainfeld, T. G. Schaaff, M. N. Shafiqullin, P. W. Stephens, and R. L. Whetten, *Eur. Phys. J. D* **9**, 647 (1999).

<sup>11</sup>H. Häkkinen, M. Moseler, O. Kostko, N. Morgner, M. A. Hoffmann, and B. v. Issendorff, *Phys. Rev. Lett.* **93**, 093401 (2004).

<sup>12</sup>J. Li, X. Li, H. J. Zhai, and L. S. Wang, *Science* **299**, 864 (2003).

<sup>13</sup>J. M. Soler, M. R. Beltran, K. Michaelian, I. L. Garzon, P. Ordejon, D. Sanchez-Portal, and E. Artacho, *Phys. Rev. B* **61**, 5771 (2000).

<sup>14</sup>H. G. Boyen, G. Kastle, F. Weigl, B. Koslowski, C. Dietrich, P. Ziemann, J. P. Spatz, S. Riethmuller, C. Hartmann, M. Moller, G. Schmid, M. G. Garnier, and P. Oelhafen, *Science* **297**, 1533 (2002).

<sup>15</sup>M. Okumura, Y. Kitagawa, M. Haruta, and K. Yamaguchi, *Chem. Phys. Lett.* **346**, 163 (2001).

<sup>16</sup>D. H. Wells, W. N. Delgass, and K. T. Thomson, *J. Chem. Phys.*

- 117**, 10597 (2002).
- <sup>17</sup>A. L. Mackay, *Acta Crystallogr.* **15**, 916 (1962).
- <sup>18</sup>R. Arratia-Perez, A. F. Ramos, and G. L. Malli, *Phys. Rev. B* **39**, 3005 (1989).
- <sup>19</sup>L. Lamare and F. Michel-Calendini, *Int. J. Quantum Chem.* **61**, 635 (1997).
- <sup>20</sup>A. F. Ramos, R. Arratia-Perez, and G. L. Malli, *Phys. Rev. B* **35**, 3790 (1987).
- <sup>21</sup>D. J. Wales and L. J. Munro, *J. Phys. Chem.* **100**, 2053 (1996).
- <sup>22</sup>W. Fa and J. M. Dong, *Appl. Phys. Lett.* **89**, 013117 (2006).
- <sup>23</sup>L. Xiao, B. Tollberg, X. K. Hu, and L. C. Wang, *J. Chem. Phys.* **124**, 114309 (2006).
- <sup>24</sup>L. Xiao and L. C. Wang, *Chem. Phys. Lett.* **392**, 452 (2004).
- <sup>25</sup>C. M. Chang and M. Y. Chou, *Phys. Rev. Lett.* **93**, 133401 (2004).
- <sup>26</sup>H. Häkkinen, M. Moseler, and U. Landman, *Phys. Rev. Lett.* **89**, 033401 (2002).
- <sup>27</sup>P. Koskinen, H. Hakkinen, B. Huber, B. von Issendorff, and M. Moseler, *Phys. Rev. Lett.* **98**, 015701 (2007).
- <sup>28</sup>N. D. Mermin, *Phys. Rev.* **137**, 1441 (1965).
- <sup>29</sup>M. Methfessel and A. T. Paxton, *Phys. Rev. B* **40**, 3616 (1989).
- <sup>30</sup>J. M. Soler, E. Artacho, J. D. Gale, A. Garcia, J. Junquera, P. Ordejon, and D. Sanchez-Portal, *J. Phys.: Condens. Matter* **14**, 2745 (2002).
- <sup>31</sup>J. P. Perdew, K. Burke, and M. Ernzerhof, *Phys. Rev. Lett.* **77**, 3865 (1996).
- <sup>32</sup>N. Troullier and J. L. Martins, *Phys. Rev. B* **43**, 1993 (1991).
- <sup>33</sup>N. Troullier and J. L. Martins, *Phys. Rev. B* **43**, 8861 (1991).
- <sup>34</sup>P. E. Blöchl, *Phys. Rev. B* **50**, 17953 (1994).
- <sup>35</sup>G. Kresse and J. Furthmüller, *Comput. Mater. Sci.* **6**, 15 (1996).
- <sup>36</sup>G. Kresse and J. Furthmüller, *Phys. Rev. B* **54**, 11169 (1996).
- <sup>37</sup>G. Kresse and J. Hafner, *Phys. Rev. B* **47**, 558 (1993).
- <sup>38</sup>G. Kresse and J. Hafner, *Phys. Rev. B* **49**, 14251 (1994).
- <sup>39</sup>G. Kresse and D. Joubert, *Phys. Rev. B* **59**, 1758 (1999).
- <sup>40</sup>M. J. Frisch, G. W. Trucks, H. B. Schlegel, G. E. Scuseria, M. A. Robb, J. R. Cheeseman, V. G. Zakrzewski, J. A. Montgomery, Jr., R. E. Stratmann, J. C. Burant, S. Dapprich, J. M. Millam, A. D. Daniels, K. N. Kudin, M. C. Strain, O. Farkas, J. Tomasi, V. Barone, M. Cossi, R. Cammi, B. Mennucci, C. Pomelli, C. Adamo, S. Clifford, J. Ochterski, G. A. Petersson, P. Y. Ayala, Q. Cui, K. Morokuma, P. Salvador, J. J. Dannenberg, D. K. Malick, A. D. Rabuck, K. Raghavachari, J. B. Foresman, J. Cioslowski, J. V. Ortiz, A. G. Baboul, B. B. Stefanov, G. Liu, A. Liashenko, P. Piskorz, I. Komaromi, R. Gomperts, R. L. Martin, D. J. Fox, T. Keith, M. A. Al-Laham, C. Y. Peng, A. Nanayakkara, M. Challacombe, P. M. W. Gill, B. Johnson, W. Chen, M. W. Wong, J. L. Andres, C. Gonzalez, M. Head-Gordon, E. S. Replogle, and J. A. Pople, *GAUSSIAN98*, Gaussian, Inc., Pittsburgh, PA, 2001.
- <sup>41</sup>M. P. Allen and D. J. Tildesley, *Computer Simulations of Liquids* (Oxford University Press, Oxford, 1987).
- <sup>42</sup>H. A. Jahn and E. Teller, *Proc. R. Soc. London, Ser. A* **161**, 220 (1937).
- <sup>43</sup>R. W. Warren and B. I. Dunlap, *Chem. Phys. Lett.* **262**, 384 (1996).
- <sup>44</sup>P. Fuentealba, H. Preuss, H. Stoll, and L. Vonszentpaly, *Chem. Phys. Lett.* **89**, 418 (1982).
- <sup>45</sup>P. J. Hay and W. R. Wadt, *J. Chem. Phys.* **82**, 299 (1985).
- <sup>46</sup>P. J. Hay and W. R. Wadt, *J. Chem. Phys.* **82**, 270 (1985).
- <sup>47</sup>W. R. Wadt and P. J. Hay, *J. Chem. Phys.* **82**, 284 (1985).
- <sup>48</sup>B. S. de Bas, M. J. Ford, and M. B. Cortie, *J. Phys.: Condens. Matter* **18**, 55 (2005).
- <sup>49</sup>J. P. Perdew and Y. Wang, *Phys. Rev. B* **45**, 13244 (1992).
- <sup>50</sup>J. P. Perdew and Y. Wang, *Phys. Rev. B* **46**, 12947 (1992).
- <sup>51</sup>A. D. Becke, *J. Chem. Phys.* **98**, 5648 (1993).